

Dynamic Traceback Learning for Medical Report Generation

Shuchang Ye

School of Computer Science
The University of Sydney
Sydney, New South Wales, Australia
shuchang.ye@sydney.edu.au

Mingjian Li

School of Computer Science
The University of Sydney
Sydney, New South Wales, Australia
mili3287@uni.sydney.edu.au

Usman Naseem

School of Computing
Macquarie University
Sydney, New South Wales, Australia
usman.naseem@mq.edu.au

Mingyuan Meng

School of Computer Science
The University of Sydney
Sydney, New South Wales, Australia
mmen2292@uni.sydney.edu.au

Dagan Feng

School of Computer Science
The University of Sydney
Sydney, New South Wales, Australia
dagan.feng@sydney.edu.au

Jinman Kim

School of Computer Science
The University of Sydney
Sydney, New South Wales, Australia
jinman.kim@sydney.edu.au

Abstract

Automated medical report generation has the potential to significantly reduce the workload associated with the time-consuming process of medical reporting. Recent generative representation learning methods have shown promise in integrating vision and language modalities for medical report generation. However, when trained end-to-end and applied directly to medical image-to-text generation, they face two significant challenges: i) difficulty in accurately capturing subtle yet crucial pathological details, and ii) reliance on both visual and textual inputs during inference, leading to performance degradation in zero-shot inference when only images are available. To address these challenges, this study proposes a novel multi-modal dynamic traceback learning framework (**DTrace**)¹. Specifically, we introduce a traceback mechanism to supervise the semantic validity of generated content and a dynamic learning strategy to adapt to various proportions of image and text input, enabling text generation without strong reliance on the input from both modalities during inference. The learning of cross-modal knowledge is enhanced by supervising the model to recover masked semantic information from a complementary counterpart. Extensive ex-

periments conducted on two benchmark datasets, IU-Xray and MIMIC-CXR, demonstrate that the proposed **DTrace** framework outperforms state-of-the-art methods for medical report generation.

1. Introduction

Medical report generation is a crucial component of the diagnostic process, providing detailed textual descriptions of medical images, which guide clinical decision-making and treatment planning [19]. However, the task of interpreting medical images and composing reports is both time-consuming and resource-intensive. Therefore, automating the report generation process has garnered significant attention as a potential solution to reduce radiologist workload [39]. Despite advances in deep learning, medical report generation remains challenging due to the difficulty in accurately associating subtle yet critical diagnostic features in medical images with their corresponding textual reports. This is because medical images often contain subtle regions, such as tumor areas, which are essential for diagnosis, while medical reports rely on a limited set of keywords to represent this diagnostic information. Hence, it is crucial to develop a method that can capture and associate this nuanced information to preserve the intrinsic medical meanings within medical images and reports.

¹Our code is provided in supplementary materials and will be publicly available on GitHub upon publication.

2. Related Work

2.1. Medical Report Generation

Traditional medical report generation methods rely on rule- or template-based methods [1]. Rule-based methods often fall short in handling different scenarios and capturing language subtleties, while template-based methods are dependent on template quality and adaptability. With the paradigm shift in Computer Vision (CV) and Natural Language Processing (NLP), deep learning-based medical report generation methods have achieved promising performance and attained wide attention [19].

Deep learning-based report generation can be traced back to the invention of encoder-decoder architecture. Within this framework, images were transmuted into representative vectors encapsulating salient information through a visual encoder, followed by a linguistic decoder to predict text [31]. Subsequent studies primarily focused on enhancing the capabilities of the visual encoder and the linguistic decoder [25], e.g., from Convolutional Neural Networks (CNN) and Recurrent Neural Networks (RNN) to Vision Transformer (ViT) and Transformer [34]. Recently, the interaction and communication between the visual encoder and linguistic decoder have also attracted wide attention. Visual language pretraining (VLP) has significantly advanced image-to-text generation tasks by effectively integrating visual and textual data. For instance, MCGN [35] employs CLIP [23] to harness contrastive learning for refining the latent space, thus boosting semantic similarity between image-text pairs. However, VLP approaches predominantly focus on training encoders, which, for tasks like report generation where decoders are equally crucial, necessitates the incorporation of additional methodologies to train both network components effectively. In medical report generation, R2GenCMN [3] proposed to unify the visual and linguistic representations by sharing a vector pool across the visual encoder and linguistic decoder. XProNet [32] further improved the R2GenCMN by monitoring the vector pool with pathological labels. These methods improved cross-modal communication and achieved state-of-the-art medical report generation performance. However, they still relied on a unidirectional image-to-report mapping and ignored the bidirectional mutual image-report associations. Recent studies have introduced additional annotations to strengthen the relationship between images and their corresponding reports. COMG [28] incorporates segmentation masks of organs to guide the model’s attention toward critical regions. Similarly, RGRG [26] integrates bounding boxes and links them to their associated sentences, enabling the model to focus more effectively on specific anatomical regions during report generation.

2.2. Generative Representation Learning

GRL methods learn the latent space representations by training the model to reconstruct the masked inputs based on the unmasked information. Masked Image Modeling (MAE) [9] and Masked Language Modeling (BERT) [6] are prevalent pre-training techniques in CV and NLP. BERT learned the word latent representations by training the model to predict the masked content based on the surrounding words. Then, MAE employed a similar strategy in images, where the images were split into patches and the model was trained to reconstruct the randomly masked patches. Recently, M3AE [8] exploited multi-modal learning and generation, where image and text reconstruction were jointly performed with a multi-modal masked encoder-decoder framework to enhance the comprehension of cross-modal associations. These GRL methods were widely adopted as a pre-training step to enhance the performance of downstream tasks, such as disease classification [36] and medical visual question answering [2].

The capability of reconstructing masked text provides the potential for report generation. However, GRL methods were seldom applied to medical report generation due to the two drawbacks that we identified above. Recently, MedViLL [20] applied GRL framework to medical report generation (as one of the downstream tasks) by progressively replacing mask tokens with predicted language tokens. Unfortunately, its performance was limited (0.066 in BLEU4 in the MIMIC-CXR dataset) as it was not trained to handle situations where text information is not available.

In contrast, our proposed framework differs in several key aspects: i) GRL methods are typically designed for pre-training on large datasets followed by fine-tuning for specific tasks, whereas our framework is trained end-to-end and can be directly applied to medical report generation; ii) GRL usually employs a fixed mask ratio, but we utilize a dynamic mask ratio; and iii) while conventional methods prioritize morphological similarity, our approach emphasizes semantic similarity.

3. Method

3.1. Network Architecture

DTrace consists of five key components: a visual encoder, a visual decoder, a linguistic encoder, a linguistic decoder, and a cross-modal fusion module (Fig. 3). The visual encoder processes partially masked images to extract incomplete pathological information. Simultaneously, the linguistic encoder also processes fragmented textual information to extract incomplete pathological information. Then, the extracted information is fed into the cross-modal fusion module, where a cross-attention mechanism is employed to foster the interaction between the visual and linguistic domains, thereby ameliorating the semantic deficits in both

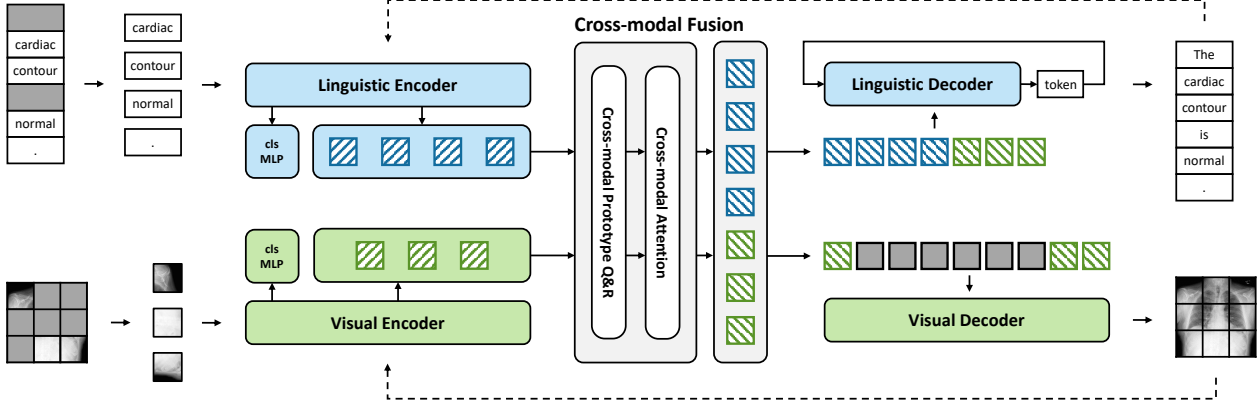


Figure 3. DTrace with dynamic traceback learning. Solid and dashed lines indicate forward and traceback stages.

modalities. After this, the enriched information is conveyed to the visual and linguistic decoders to restore the masked images and reports to their original unmasked states. Below, we discuss the key components of DTrace in detail:

Visual Encoder is consistent with the common practice of MAE; medical images were split into patches and then randomly masked. The visual encoder was a standard ViT [7], which mapped the unmasked patches into latent representations and then performed multi-label classification to predict the disease labels extracted via CheXbert [24]. In **Linguistic Encoder**, medical reports were mapped into embedded text tokens following the standard pre-processing steps [6]. Then, these tokens were randomly masked and fed into the linguistic encoder. The linguistic encoder was a classic text transformer block [29]. For the **Cross-Modal Fusion Module**, the features extracted from both the encoders were projected to a pre-defined dimension, which then was then concatenated and fed to a cross-modal attention module [8] for information interchange. The resultant features were subsequently separated and mapped into latent representations via Multi-layer Perceptrons (MLPs) [27]. In **Visual Decoder**, the masked tokens were reinstated to their original positions, aligning with the unmasked encoding tokens. Following this, a lite version of ViT [9] was used to restore the masked patches. For the **Linguistic Decoder**, We adopted a relational memory Transformer [4] to perform report generation. Taking previously generated text as the value, the decoder treated the concatenation of image patches and text patches as the query and key of the self-attention module to predict the next subsequent word.

3.2. Traceback Mechanism

The traceback mechanism (Fig. 4) was developed to ensure the medical validity of generated outputs through two phases: forward and traceback. Initially, encoder capabilities are enhanced to identify pathological information dur-

ing the forward phase. Subsequently, the decoder outputs are redirected to their corresponding encoders in the traceback stage to check their medical validity. Through repetitive iterations between the two stages, the DTrace model enhances accuracy by refining its understanding of medical content, ensuring reliable identification and validation of pathological information in image reconstruction and report generation.

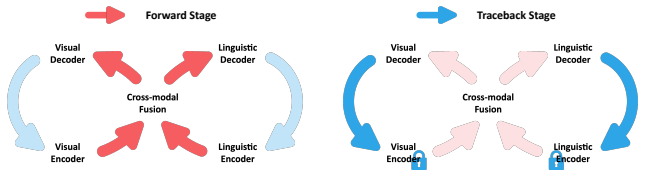


Figure 4. Dynamic traceback learning with forward stage (left) and traceback stage (right). The lock means that there is no gradient descent in back-propagation.

3.3. Dynamic Learning Strategy

Existing multi-modal GRL methods incurred performance degradation when generating reports from images alone. To address this limitation, the dynamic learning strategy was proposed to enhance the generalizability of the model to perform multi-modal generation given any percentage of text and image inputs. This was achieved through training with various complementary image and text mask ratios (different mask ratios for each batch). This complementary relation aimed to guarantee sufficient shared information and to ensure that each modality can consistently derive some information from the other. It also incorporated a self-adjustment mechanism for loss weights, dynamically adapting to changes in the mask ratios. The pseudo-code of the dynamic traceback learning is shown in Algorithm 1. In the subsequent sections, the mathematical rationale behind the adjustment of loss weights during the forward and traceback stages is presented.

Algorithm 1 Dynamic Traceback Learning

```
1: Generate random numbers:  $\alpha$  as image mask ratio and  
    $\beta = 1 - \alpha$  as text mask ratio  
2: while Not reach max epoch and early stop do  
3:   if Forward then  
4:     imasked, tmasked  $\leftarrow$  masking(image, text)  
5:     ifeats, tfeats  $\leftarrow$  encoders(imasked, tmasked)  
6:     compute  $\ell_{FVD}$  and  $\ell_{FLD}$   
7:     gradient descent encoders by  $(1 - \alpha) \cdot \ell_{FVD}$  and  
        $(1 - \beta) \cdot \ell_{FLD}$   
8:     feats  $\leftarrow$  cross modal fusion(ifeats, tfeats)  
9:     igen, tgen  $\leftarrow$  decoders(feats)  
10:    compute  $\ell_{IR}$  and  $\ell_{RG}$   
11:    gradient descent all components by  $\alpha \cdot \ell_{IR}$  and  $\beta \cdot$   
        $\ell_{RG}$   
12:   end if  
13:   if Traceback then  
14:     disable the gradient descent of encoders  
15:     igfeats, tgfacts  $\leftarrow$  encoders(igen, tgen)  
16:     compute  $\ell_{TVD}$  and  $\ell_{TLD}$   
17:     gradient descent all except encoders by  $\alpha \cdot$   
        $e^{-\ell_{FVD}} \ell_{TVD}$  and  $\beta \cdot e^{-\ell_{FLD}} \ell_{TLD}$   
18:   end if  
19: end while
```

Assumed the mask ratio of images to be a random number $0 \leq \alpha \leq 1$. The corresponding mask ratio of reports would then be $\beta = 1 - \alpha$.

Forward Stage The forward stage of the DTrace model performs three main tasks: 1) disease identification by the encoders, 2) image reconstruction by the visual decoder, and 3) report generation by the linguistic decoder, as shown in the left of Fig. 4.

For disease identification, we integrated a multi-label classification head for N classes into the encoders to predict disease labels as output. According to the dynamic learning strategy, the image and reports are masked in the forward stage based on the dynamic complementary mask ratio. Subsequently, the remaining unmasked components are directed to their respective encoders. To optimize the generation of their corresponding label outputs, both the encoders aim to minimize the diagnostic loss. The diagnostic loss is the binary cross-entropy (BCE) loss (see Equation 1) between the instances of disease label extracted by CheXbert, y and the encoders' corresponding predicted label, \hat{y} . As a diagnosis can only be meaningful when sufficient unmasked information is available, the visual and linguistic encoders' respective diagnostic losses complement their corresponding image and text mask ratios. The resulting forward visual diagnostic (FVD) loss and forward linguistic diagnostic (FLD) loss are shown in Equation 2 and Equation 3.

$$\ell_{BCE}(y, \hat{y}) = -\frac{1}{N} \sum_{i=1}^N y_i \cdot \log(\hat{y}_i) + (1 - y_i) \cdot \log(1 - \hat{y}_i) \quad (1)$$

$$\ell_{FVD}(y, \hat{y}) = (1 - \alpha) \cdot \ell_{BCE}(y, \hat{y}) \quad (2)$$

$$\ell_{FLD}(y, \hat{y}) = (1 - \beta) \cdot \ell_{BCE}(y, \hat{y}) \quad (3)$$

For image reconstruction, we follow the MAE's practice [9] in that the visual decoder takes the visual features that gained knowledge from the cross-model fusion module and learned vector that indicated the presence of the masked patch as input. The image reconstruction process is regulated through minimizing the image reconstruction (IR) loss, which is the pixel-wise mean-square-error (MSE) weighted proportional to the image mask ratio to facilitate cross-modal communication, as shown in Equation 4. In Equation 4, g represents an instance of the origin image and \hat{g} represents the respective reconstructed image, and W and H represent the width and height of the image, respectively.

$$\ell_{IR}(g, \hat{g}) = \alpha \cdot \frac{1}{W} \frac{1}{H} \sum_{i=1}^W \sum_{j=1}^H (g_{ij} - \hat{g}_{ij})^2 \quad (4)$$

The generated reports are refined by minimizing the report generation (RG) loss. The RG loss, as shown in Equation 5, is the word-level cross-entropy (CE) loss weighted corresponding to the text mask ratio to attend to instances where reports are generated solely from images, where r represents an instance of ground truth report, \hat{r} represents the corresponding generated report, V represents the vocabulary size and L represents the report length.

$$\ell_{RG}(r, \hat{r}) = \beta \cdot \frac{1}{V} \frac{1}{L} \sum_{i=1}^V \sum_{j=1}^L r_{ij} \cdot \log\left(\frac{e^{\hat{r}_{ij}}}{\sum_{k=1}^V e^{\hat{r}_{ik}}}\right) \quad (5)$$

Traceback Stage As depicted in the right of Fig. 4, the images reconstructed and reports generated by the decoders were traced back to be the input of **locked** encoders. The encoders inference on both the reconstructed items ($\hat{\tilde{y}}$) and unmasked items (\tilde{y}). However, this principle was heavily dependent on the accuracy of the encoders, which led to significant fluctuations in the early stages of training. This problem was addressed by introducing a compensation mechanism: the weights of traceback losses were inversely proportional to the losses of the generation process, as shown in Equation 6 and Equation 7.

$$\ell_{TVD}(\tilde{y}, \hat{\tilde{y}}) = \alpha \cdot e^{-\ell_{FVD}(\tilde{y}, \hat{\tilde{y}})} \cdot \ell_{BCE}(\tilde{y}, \hat{\tilde{y}}) \quad (6)$$

$$\ell_{TLD}(\tilde{y}, \hat{\tilde{y}}) = \alpha \cdot e^{-\ell_{FLD}(\tilde{y}, \hat{\tilde{y}})} \cdot \ell_{BCE}(\tilde{y}, \hat{\tilde{y}}) \quad (7)$$

4. Experimental Setup

4.1. Dataset

We conducted experiments on two well-benchmarked public datasets, Indiana University Chest X-ray (IU-Xray) [5] and MIMIC Chest X-ray (MIMIC-CXR) [12]. We split the data into training, validation, and testing subsets. For IU-Xray, we adopt the widely accepted 7:1:2 data split as suggested in prior studies [3, 4, 32]. For MIMIC-CXR, we adhere to the official data split.

4.2. Evaluation Metrics

To measure the quality of generated medical report, we follow the standard practice [3, 4, 32, 34] to adopt natural language generation (NLG) metrics: BLEU [21], METEOR [13], ROUGE-L [15], and CIDEr [30] as the evaluation metrics. We further assess the clinical efficacy (CE) [3, 4, 10, 11] of the generated reports by annotating them with CheXbert and comparing the predicted and ground truth labels.

4.3. Baselines

We compared the performance of DTrace against the state-of-the-art medical report generation methods (see Section 5.1): R2Gen [4], R2GenCMN [3], CMCL [16], AlignTransformer [38], XProNet [32], MCTransformer [34], M2KT [37], ORGAN [10] and KiUT [11]. For fair evaluation, the released code from the baseline methods was used in the same settings as described in the papers. Please see appendix A.1 for implementation details.

5. Result and Analysis

5.1. Comparisons to Previous Methods

Table 1 presents a comprehensive comparison with state-of-the-art methods, highlighting the superior performance of the proposed DTrace across both NLG and clinical efficacy (CE) metrics on the IU-Xray and MIMIC-CXR datasets. DTrace consistently ranks among the top performers in NLG metrics, particularly excelling in BLEU-3, BLEU-4, and CIDEr, which underscores its strong capability in generating morphologically accurate and linguistically coherent reports. In terms of CE metrics, DTrace achieves the best results in recall and F1-score and the second-best in precision, demonstrating its effectiveness in capturing disease regions and generating semantically meaningful reports. Even in comparison with models like COMG and RGRG, which leverage additional segmentation masks and region-specific information, DTrace remains highly competitive.

This superior performance suggests that DTrace is adept at capturing pathology-critical information, making it well-suited for scenarios where radiologists’ descriptions of the

same radiology image vary in writing style and terminology. For example, when comparing the ground truth sentence “the heart size is normal” with two variants, “the heart size is enlarged” and “the heart size is within normal limits,” the cross-entropy is smaller for the first variant. To address this potential bias towards common phrasing, which might sacrifice semantic accuracy, we introduce a traceback mechanism. This mechanism evaluates generated reports using an encoder trained for accurate diagnosis, thus reinforcing semantic correctness and diluting the impact of cross-entropy loss.

The proposed DTrace outperforms models such as R2GenCMN, AlignTransformer, and XProNet, which we attribute to the benefits of multi-modal learning, particularly in facilitating cross-modal communication. The traceback mechanism further contributes to this performance improvement. Even when a modality lacks information from another, it can reconstruct its form independently, while the traceback mechanism ensures that semantic information is still obtained from another modality. In the cross-modal fusion module, different modalities exchange and complement each other’s information, thereby establishing a robust communication protocol. This approach achieves effects similar to R2GenCMN and XProNet, with the added enhancement of the traceback mechanism, leading to overall improved performance.

5.2. Ablation Study

The ablation study results presented in Table 2 demonstrate the contribution of each individual component to the overall performance of DTrace. Below, we provide a concise discussion of the impact of each component of DTrace. **Bi-directional Multi-modal Generation:** Incorporating bi-directional generation significantly improved the model’s ability to capture mutual associations between medical images and their corresponding reports. This enhancement led to a notable increase in CIDEr, from 0.143 to 0.241, and a slight improvement in the F1 score to 0.280. The bi-directional nature of the approach allows the model to better align the content of the generated reports with visual features, thereby improving both the relevance and accuracy of the textual output.

Dynamic Learning: The introduction of dynamic learning resulted in a significant performance boost across all metrics, particularly in BLEU-4, which increased from 0.107 to 0.120, and the F1 score, which rose to 0.344. This component’s ability to adapt to varying proportions of image and text inputs enabled the model to generate more contextually accurate reports without over-reliance on one modality.

Traceback Mechanism: The traceback mechanism provided the most substantial improvements. By supervising the semantic validity of the generated content, this component enhanced the model’s ability to produce clinically ac-

Table 1. Performance comparison between DTrace and existing report generation methods on the IU-Xray and MIMIC-CXR datasets. The best results are highlighted in bold and the second best are underlined. BL, MTR, RG-L and CDr are the abbreviations of NLG evaluation metrics BLEU, METEOR, ROUGE-L and CIDEr. P, R, F are the abbreviations of CE metrics: Precision, Recall, F1-score. Gray indicates the utilization of additional annotations. * denotes that the results are cited from their original papers.

Dataset	Model	BL-1	BL-2	BL-3	BL-4	MTR	RG-L	CDr	P	R	F
IU-Xray	R2Gen	0.470	0.304	0.211	0.157	0.197	0.364	0.342	-	-	-
	R2GenCMN	0.486	0.307	0.216	0.156	0.212	0.374	0.331	-	-	-
	CMCL*	0.473	0.305	0.217	0.162	0.186	0.378	-	-	-	-
	AlignTransformer*	0.484	0.313	0.225	0.173	0.204	0.379	-	-	-	-
	MCTransformer*	0.496	0.319	0.241	0.175	-	0.377	<u>0.449</u>	-	-	-
	M2KT*	0.497	0.319	0.230	0.174	-	0.399	0.407	-	-	-
	ORGAN*	0.494	0.335	0.247	<u>0.190</u>	0.203	<u>0.395</u>	-	-	-	-
	KiUT	0.525	0.360	<u>0.251</u>	0.185	0.242	0.409	-	-	-	-
	DTrace (ours)	<u>0.516</u>	<u>0.353</u>	0.278	0.204	<u>0.233</u>	<u>0.386</u>	0.469	-	-	-
	COMG*	0.482	0.316	0.233	0.184	0.191	0.382	-	-	-	-
MIMIC-CXR	R2Gen	0.344	0.208	0.140	0.100	0.135	0.271	0.146	0.333	0.273	0.276
	R2GenCMN	0.327	0.211	0.148	0.109	0.137	<u>0.298</u>	0.135	0.334	0.275	0.278
	CMCL*	0.344	0.217	0.140	0.097	0.133	0.281	-	-	-	-
	AlignTransformer*	0.378	0.235	0.156	0.112	0.158	0.283	-	-	-	-
	MCTransformer*	0.351	0.223	0.157	0.118	-	0.287	<u>0.281</u>	-	-	-
	M2KT*	0.386	0.237	0.157	0.111	-	0.274	0.111	-	-	-
	ORGAN*	0.405	<u>0.254</u>	<u>0.170</u>	<u>0.121</u>	<u>0.161</u>	0.291	-	0.416	<u>0.418</u>	<u>0.385</u>
	KiUT	0.393	0.243	0.159	0.113	0.160	0.285	-	0.371	0.318	0.321
	DTrace (ours)	<u>0.392</u>	0.260	0.171	0.129	0.162	0.309	0.311	<u>0.411</u>	0.436	0.391
	COMG*	0.346	0.216	0.145	0.104	0.137	0.279	-	0.424	0.291	0.345
RGRG	0.373	0.249	0.175	0.126	0.168	0.264	0.495	0.461	0.475	0.447	

Table 2. Ablation study on key components of our proposed DTrace on MIMIC-CXR dataset.

Model	BL-1	BL-2	BL-3	BL-4	MTR	RG-L	CDr	P	R	F
Uni-modal Report Auto-completion	0.351	0.215	0.141	0.102	0.133	0.264	0.108	0.277	0.244	0.236
Encoder-Decoder (Baseline)	0.348	0.212	0.143	0.106	0.136	0.277	0.143	0.325	0.271	0.268
+ Bi-directional Generation	0.346	0.220	0.144	0.107	0.142	0.285	0.241	0.345	0.280	0.280
+ Dynamic Learning	0.371	0.243	0.165	0.120	0.155	0.281	0.279	0.358	0.355	0.344
+ Traceback Mechanism	0.392	0.260	0.171	0.129	0.162	0.309	0.311	0.411	0.436	0.391
Multi-modal Masked Autoencoder	0.364	0.246	0.164	0.119	0.153	0.284	0.292	0.354	0.296	0.301

curate and coherent reports. The BLEU-4 score increased to 0.129, while CIDEr reached 0.311, indicating improved alignment with the true medical meaning of the reports. Clinically, the model achieved a precision of 0.411, recall of 0.436, and an F1 score of 0.391. These improvements underscore the traceback mechanism’s critical role in ensuring that the generated text not only follows the expected structure but also conveys accurate and meaningful clinical information.

Understanding of Cross-modal Knowledge: The DTrace framework demonstrates clear superiority over both the baseline Encoder-Decoder model and the Multi-modal

Masked Autoencoder. While the baseline model struggles to generate clinically accurate reports, often relying on statistical regularities, DTrace’s dynamic learning strategy and traceback mechanism ensure that the generated content is both semantically valid and clinically meaningful. Compared to the Multi-modal Masked Autoencoder, which integrates vision and language modalities but faces challenges in maintaining semantic precision, DTrace excels by dynamically adapting to varying input proportions and supervising the clinical relevance of the generated content.

Table 3. Comparison of the traditional fixed mask ratio training strategy versus our dynamic learning strategy on the IU-Xray dataset, with our method highlighted in bold.

Strategy	Mask Ratio	BL-1	BL-2	BL-3	BL-4	MTR	RG-L	CDr
Fixed	0%	0.397	0.255	0.183	0.139	0.164	0.367	0.364
	15%	0.441	0.284	0.207	0.158	0.180	0.378	0.427
	30%	0.459	0.293	0.207	0.155	0.176	0.368	0.255
	45%	0.465	0.299	0.211	0.155	0.176	0.367	0.289
	60%	0.468	0.300	0.214	0.159	0.196	0.382	0.308
	75%	0.479	0.307	0.221	0.164	0.195	0.385	0.364
Dynamic	varying	0.516	0.353	0.278	0.204	0.233	0.386	0.469

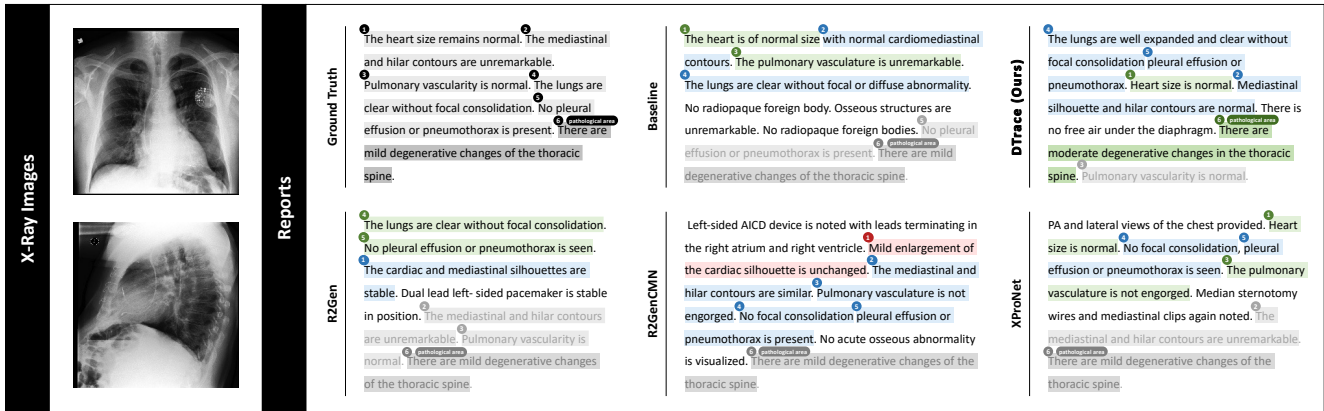


Figure 5. An example (patient 10014765) of comparisons between different report generation frameworks and the proposed DTrace framework. The information in the ground truth report is labeled from 1 to 6 and highlighted separately. The generated reports are labeled according to the ground truth report and highlighted with different colors to represent the differences between the generated sequences and the ground truth report: (1) Green - consistent; (2) Blue - semantically similar but different in expression; (3) Pink - incorrect information; (4) Gray - missing sentences; (5) Unhighlighted - not included in the ground truth.

5.3. Impact of Mask Ratios

To illustrate the significance of dynamic learning in medical report generation, we compared traditional methods that use a fixed mask ratio with our proposed method, which employs a varying mask ratio, as shown in Table 3. Our comparison revealed that the model’s performance improves as the mask ratio increases. Importantly, during training, the model is exposed to both image and text data, whereas, during inference, it processes only the image data. The greater the discrepancy between the information available during training and inference, the worse the model’s performance tends to be. Our dynamic learning approach effectively mitigates this issue by randomly varying the proportions of information from both modalities, thus enhancing the model’s robustness during inference.

5.4. Qualitative Analysis and Visualization

We conducted a qualitative analysis of DTrace compared to the baseline encoder-decoder framework. As illustrated in Fig. 5, when dealing with rare diseases, the baseline and

existing methods frequently omit critical diagnostic statements, such as ”mild degenerative changes in the thoracic spine,” despite having a high degree of textual overlap with the ground truth. In contrast, the DTrace-generated reports include most of the essential diagnostic statements and demonstrate a high level of consistency with the ground-truth reports. Additionally, Fig. A3 presents images reconstructed from 75%-masked images and unmasked reports by DTrace. These reconstructed images exhibit a high degree of consistency with the original unmasked images, highlighting DTrace’s effectiveness in image reconstruction. Further visualizations can be found in the supplementary materials.

We further assessed the morphological and semantic similarities between the constructed images and the original images. To evaluate the efficacy of our dynamic traceback learning in reducing pixel-level differences, we conducted a control experiment comparing the quality of images generated with and without dynamic traceback learning, as depicted in Fig. A1. Our analysis revealed a distinct

boundary between generated patches and original patches in images not reconstructed using the dynamic traceback learning strategy. Although dynamic traceback learning is not specifically designed to enhance morphological similarity, the images reconstructed using this method appear more cohesive and clearer.

To quantify the quality of the generated images, we compared the Frechet Inception Distance (FID) scores. After implementing dynamic traceback learning, the FID of the constructed images decreased from 166.4 to 98.6, indicating that dynamic traceback learning more accurately mimics the distribution of the original images and produces higher-quality, more realistic reconstructions. Additionally, we employed a classification evaluation method to assess the semantic correctness of the reconstructed images. Table A1 demonstrates that DTrace successfully reconstructs images from 75%-masked images and unmasked text input while preserving semantic information.

6. Conclusion

In this study, we introduced a novel medical report generation framework, DTrace, which leverages multi-modal dynamic traceback learning. We incorporated a traceback mechanism to ensure semantic correctness during training and a dynamic learning strategy to reduce the dependency of existing generative cross-modal frameworks on textual input. Our experimental results demonstrated that both the traceback mechanism and the dynamic learning strategy significantly enhance the multi-modal generation framework, enabling DTrace to achieve state-of-the-art performance on the well-benchmarked IU-Xray and MIMIC-CXR datasets.

References

- [1] Alison J Cawsey, Bonnie L Webber, and Ray B Jones. Natural language generation in health care. *Journal of the American Medical Informatics Association*, 4(6):473–482, 1997. 3
- [2] Zhihong Chen, Yuhao Du, Jinpeng Hu, Yang Liu, Guanbin Li, Xiang Wan, and Tsung-Hui Chang. Multi-modal masked autoencoders for medical vision-and-language pre-training. In *International Conference on Medical Image Computing and Computer-Assisted Intervention*, pages 679–689. Springer, 2022. 3
- [3] Zhihong Chen, Yaling Shen, Yan Song, and Xiang Wan. Cross-modal memory networks for radiology report generation. In *Proceedings of the 59th Annual Meeting of the Association for Computational Linguistics and the 11th International Joint Conference on Natural Language Processing (Volume 1: Long Papers)*, pages 5904–5914, Online, Aug. 2021. Association for Computational Linguistics. 3, 6
- [4] Zhihong Chen, Yan Song, Tsung-Hui Chang, and Xiang Wan. Generating radiology reports via memory-driven transformer. In *Proceedings of the 2020 Conference on Empirical Methods in Natural Language Processing*, Nov. 2020. 2, 4, 6
- [5] Dina Demner-Fushman, Marc Kohli, Marc Rosenman, Sonya Shooshan, Laritza Rodriguez, Sameer Antani, George Thoma, and Clement McDonald. Preparing a collection of radiology examinations for distribution and retrieval. *Journal of the American Medical Informatics Association : JAMIA*, 23, 07 2015. 6
- [6] Jacob Devlin, Ming-Wei Chang, Kenton Lee, and Kristina Toutanova. Bert: Pre-training of deep bidirectional transformers for language understanding. *arXiv preprint arXiv:1810.04805*, 2018. 2, 3, 4
- [7] Alexey Dosovitskiy, Lucas Beyer, Alexander Kolesnikov, Dirk Weissenborn, Xiaohua Zhai, Thomas Unterthiner, Mostafa Dehghani, Matthias Minderer, Georg Heigold, Sylvain Gelly, et al. An image is worth 16x16 words: Transformers for image recognition at scale. *arXiv preprint arXiv:2010.11929*, 2020. 4
- [8] Xinyang Geng, Hao Liu, Lisa Lee, Dale Schuurmans, Sergey Levine, and Pieter Abbeel. Multimodal masked autoencoders learn transferable representations. *arXiv preprint arXiv:2205.14204*, 2022. 2, 3, 4
- [9] Kaiming He, Xinlei Chen, Saining Xie, Yanghao Li, Piotr Dollár, and Ross Girshick. Masked autoencoders are scalable vision learners. In *Proceedings of the IEEE/CVF conference on computer vision and pattern recognition*, pages 16000–16009, 2022. 2, 3, 4, 5
- [10] Wenjun Hou, Kaishuai Xu, Yi Cheng, Wenjie Li, and Jiang Liu. Organ: Observation-guided radiology report generation via tree reasoning. *arXiv preprint arXiv:2306.06466*, 2023. 6
- [11] Zhongzhen Huang, Xiaofan Zhang, and Shaoting Zhang. Kiut: Knowledge-injected u-transformer for radiology report generation. In *Proceedings of the IEEE/CVF Conference on Computer Vision and Pattern Recognition*, pages 19809–19818, 2023. 6
- [12] Alistair Johnson, Tom Pollard, Seth Berkowitz, Nathaniel Greenbaum, Matthew Lungren, Chih-ying Deng, Roger Mark, and Steven Horng. MIMIC-CXR, a de-identified publicly available database of chest radiographs with free-text reports. *Scientific Data*, 6:317, 12 2019. 6
- [13] Alon Lavie and Abhaya Agarwal. Meteor: An automatic metric for mt evaluation with high levels of correlation with human judgments. In *Proceedings of the Second Workshop on Statistical Machine Translation*, StatMT '07, page 228–231, USA, 2007. Association for Computational Linguistics. 6
- [14] Gang Li, Heliang Zheng, Daqing Liu, Chaoyue Wang, Bing Su, and Changwen Zheng. Semmae: Semantic-guided masking for learning masked autoencoders. *Advances in Neural Information Processing Systems*, 35:14290–14302, 2022. 2
- [15] Chin-Yew Lin. ROUGE: A package for automatic evaluation of summaries. In *Text Summarization Branches Out*, pages 74–81, Barcelona, Spain, July 2004. Association for Computational Linguistics. 6
- [16] Fenglin Liu, Shen Ge, and Xian Wu. Competence-based multimodal curriculum learning for medical report genera-

- tion. In *Proceedings of the 59th Annual Meeting of the Association for Computational Linguistics and the 11th International Joint Conference on Natural Language Processing (Volume 1: Long Papers)*, pages 3001–3012, Online, Aug. 2021. Association for Computational Linguistics. 6
- [17] Ilya Loshchilov and Frank Hutter. Decoupled weight decay regularization. *arXiv preprint arXiv:1711.05101*, 2017. 12
- [18] Haoyu Lu, Qiongyi Zhou, Nanyi Fei, Zhiwu Lu, Mingyu Ding, Jingyuan Wen, Changde Du, Xin Zhao, Hao Sun, Huiguang He, et al. Multimodal foundation models are better simulators of the human brain. *arXiv preprint arXiv:2208.08263*, 2022. 2
- [19] Pablo Messina, Pablo Pino, Denis Parra, Alvaro Soto, Cecilia Besa, Sergio Uribe, Marcelo Andía, Cristian Tejos, Claudia Prieto, and Daniel Capurro. A survey on deep learning and explainability for automatic report generation from medical images. *ACM Computing Surveys (CSUR)*, 54(10s):1–40, 2022. 1, 3
- [20] Jong Hak Moon, Hyungyung Lee, Woncheol Shin, Young-Hak Kim, and Edward Choi. Multi-modal understanding and generation for medical images and text via vision-language pre-training. *IEEE Journal of Biomedical and Health Informatics*, 26(12):6070–6080, 2022. 3
- [21] Kishore Papineni, Salim Roukos, Todd Ward, and Wei-Jing Zhu. Bleu: A method for automatic evaluation of machine translation. In *Proceedings of the 40th Annual Meeting on Association for Computational Linguistics, ACL '02*, page 311–318, USA, 2002. Association for Computational Linguistics. 6
- [22] Adam Paszke, Sam Gross, Francisco Massa, Adam Lerer, James Bradbury, Gregory Chanan, Trevor Killeen, Zeming Lin, Natalia Gimelshein, Luca Antiga, et al. Pytorch: An imperative style, high-performance deep learning library. *Advances in neural information processing systems*, 32, 2019. 12
- [23] Alec Radford, Jong Wook Kim, Chris Hallacy, Aditya Ramesh, Gabriel Goh, Sandhini Agarwal, Girish Sastry, Amanda Askell, Pamela Mishkin, Jack Clark, et al. Learning transferable visual models from natural language supervision. In *International conference on machine learning*, pages 8748–8763. PMLR, 2021. 3
- [24] Akshay Smit, Saahil Jain, Pranav Rajpurkar, Anuj Pareek, Andrew Y Ng, and Matthew Lungren. Combining automatic labelers and expert annotations for accurate radiology report labeling using bert. In *Proceedings of the 2020 Conference on Empirical Methods in Natural Language Processing (EMNLP)*, pages 1500–1519, 2020. 4
- [25] Matteo Stefanini, Marcella Cornia, Lorenzo Baraldi, Silvia Cascianelli, Giuseppe Fiameni, and Rita Cucchiara. From show to tell: A survey on image captioning. *arXiv preprint arXiv:2107.06912*, 2021. 3
- [26] Tim Tanida, Philip Müller, Georgios Kaissis, and Daniel Rueckert. Interactive and explainable region-guided radiology report generation. In *Proceedings of the IEEE/CVF Conference on Computer Vision and Pattern Recognition*, pages 7433–7442, 2023. 3
- [27] Hind Taud and JF Mas. Multilayer perceptron (mlp). *Geomatic approaches for modeling land change scenarios*, pages 451–455, 2018. 4
- [28] Gu Tiancheng, Liu Dongnan, Li Zhiyuan, and Cai Weidong. Complex organ mask guided radiology report generation. *arXiv preprint arXiv:2311.02329*, 2023. 3
- [29] Ashish Vaswani, Noam Shazeer, Niki Parmar, Jakob Uszkoreit, Llion Jones, Aidan N Gomez, Łukasz Kaiser, and Illia Polosukhin. Attention is all you need. *Advances in neural information processing systems*, 30, 2017. 2, 4
- [30] Ramakrishna Vedantam, C Lawrence Zitnick, and Devi Parikh. Cider: Consensus-based image description evaluation. In *Proceedings of the IEEE conference on computer vision and pattern recognition*, pages 4566–4575, 2015. 6
- [31] Oriol Vinyals, Alexander Toshev, Samy Bengio, and Dumitru Erhan. Show and tell: A neural image caption generator. In *Proceedings of the IEEE conference on computer vision and pattern recognition*, pages 3156–3164, 2015. 3
- [32] Jun Wang, Abhir Bhalerao, and Yulan He. Cross-modal prototype driven network for radiology report generation. In *European Conference on Computer Vision*, pages 563–579. Springer, 2022. 3, 6
- [33] Yixin Wang, Zihao Lin, and Haoyu Dong. Rethinking medical report generation: Disease revealing enhancement with knowledge graph. *arXiv preprint arXiv:2307.12526*, 2023. 2
- [34] Zhanyu Wang, Hongwei Han, Lei Wang, Xiu Li, and Luping Zhou. Automated radiographic report generation purely on transformer: A multicriteria supervised approach. *IEEE Transactions on Medical Imaging*, 41(10):2803–2813, 2022. 2, 3, 6
- [35] Zhanyu Wang, Mingkang Tang, Lei Wang, Xiu Li, and Luping Zhou. A medical semantic-assisted transformer for radiographic report generation. In *Medical Image Computing and Computer Assisted Intervention—MICCAI 2022: 25th International Conference, Singapore, September 18–22, 2022, Proceedings, Part III*, pages 655–664. Springer, 2022. 3
- [36] Junfei Xiao, Yutong Bai, Alan Yuille, and Zongwei Zhou. Delving into masked autoencoders for multi-label thorax disease classification. In *Proceedings of the IEEE/CVF Winter Conference on Applications of Computer Vision*, pages 3588–3600, 2023. 3
- [37] Shuxin Yang, Xian Wu, Shen Ge, Zhuozhao Zheng, S Kevin Zhou, and Li Xiao. Radiology report generation with a learned knowledge base and multi-modal alignment. *Medical Image Analysis*, 86:102798, 2023. 6
- [38] Di You, Fenglin Liu, Shen Ge, Xiaoxia Xie, Jing Zhang, and Xian Wu. Aligntransformer: Hierarchical alignment of visual regions and disease tags for medical report generation. In *Medical Image Computing and Computer Assisted Intervention—MICCAI 2021: 24th International Conference, Strasbourg, France, September 27–October 1, 2021, Proceedings, Part III 24*, pages 72–82. Springer, 2021. 2, 6
- [39] Yongxin Zhou, Fabien Ringeval, and François Portet. A survey of evaluation methods of generated medical textual reports. In Tristan Naumann, Asma Ben Abacha, Steven Bethard, Kirk Roberts, and Anna Rumshisky, editors, *Proceedings of the 5th Clinical Natural Language Processing*

Workshop, pages 447–459, Toronto, Canada, July 2023. Association for Computational Linguistics. [1](#)

A. Appendix / supplemental material

A.1. Implementation Details

Our implementation of DTrace was realized using the PyTorch package [22]. Optimization of the gradient descent process was carried out utilizing the AdamW optimizer [17], with a set learning rate of 10^{-4} . In the context of report generation, the beam search algorithm was employed, with a specified beam width of 3. The predefined maximum lengths for the reports were set at 60 and 100 for the IU-Xray and MIMIC-CXR datasets, respectively. Training of the model was performed on an NVIDIA RTX A6000 graphics card, with a designated mini-batch size of 16. To enhance the efficiency of training, the model initially underwent a pre-training phase, wherein it was conditioned to reconstruct images and reports based on the information inherent to their respective modalities, coupled with contrastive learning techniques.

B. Extended Study

B.1. Visualization and Analysis

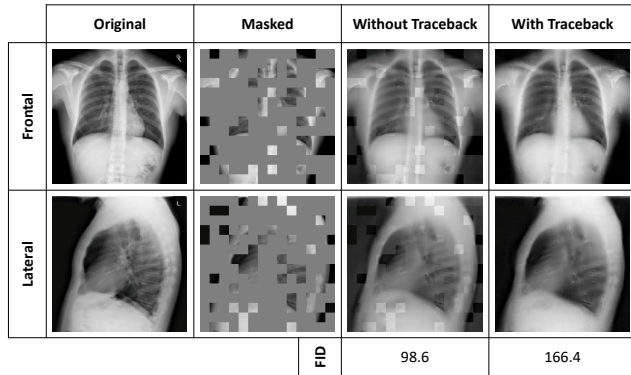


Figure A1. Comparison of visualization of reconstructed images with and without dynamic traceback learning.

Figure A1 compares the reconstruction performance of our model with and without the traceback mechanism, applied to both frontal and lateral chest X-rays. While both approaches are capable of reconstructing masked images, the traceback mechanism enhances the model’s ability to capture more intricate anatomical details, which may be essential for supporting medical interpretations.

Figure A3 illustrates the effectiveness of our model in reconstructing semantic information from medical images with a high degree of masking. Despite the significant amount of missing information in the masked images, the reconstructed images demonstrate that our model is capable of effectively recovering the essential semantic details. Notably, key anatomical features like lung structures and

Table A1. The classification performance comparison between original images and reconstructed images.

	Accuracy	Precision	Sensitivity
Original	0.861	0.922	0.904
Reconstructed	0.868	0.909	0.931

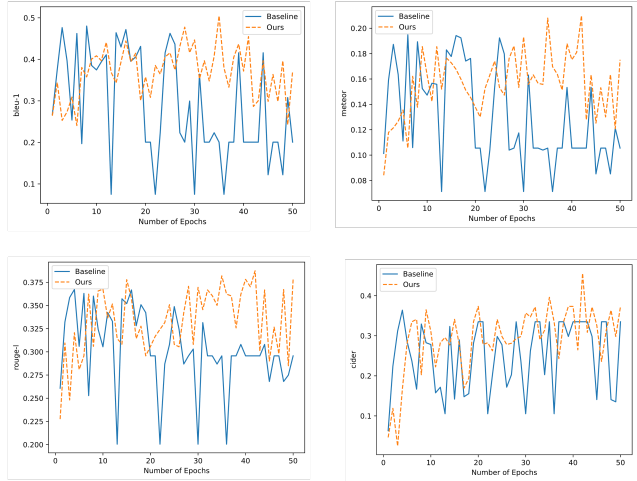


Figure A2. Comparative Visualization of Learning Process. The x-axis represents the epoch count, while the y-axis quantifies evaluation metrics (BLEU, METEOR, ROUGE-L, and CIDEr). The baseline model, featuring a traditional encoder-decoder architecture, is deline-ated by the blue line, whereas our novel framework is depicted by the orange line.

ribcage outlines are well-preserved and accurately restored. This illustrates the model’s ability to infer and reconstruct the medical context based on the available information, which aligns with the content of the associated medical reports.

B.2. Learning Process

Our investigation further delved into the model’s learning process by visualizing the evaluation metrics of the validation set as a function of epochs, as depicted in Fig. A2. We noted that traditional models for report generation exhibited considerable fluctuations in performance metrics during training and were prone to entrapment in local minima. When trapped in a local minimum, the model tended to produce “average reports,” generating identical reports for any input image, which corresponded to a relatively low cross-entropy loss. However, such models are practically futile, as this is a consequence of data imbalance and inconsistency in report expression. In cases where descriptions pertain to a specific organ, the majority of instances are deemed normal, leading the model to a complacency that precludes learning how to extract features and transmit visual information to the text generator. To minimize cross-entropy loss, the model might adopt a uniform expres-

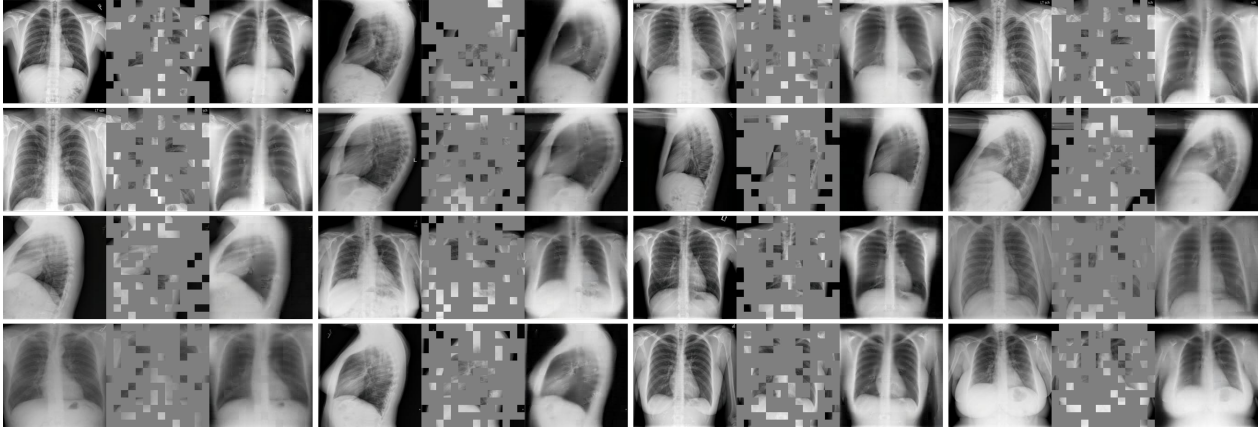


Figure A3. Visualization of the reconstructed images with a mask ratio of 75% from the model. For each triplet, we show the original image (left), the masked image (middle), and our reconstructed image (right).

sion approach. In short, traditional methods, in our context, incline the model to learn a template that minimizes cross-entropy loss, rather than diagnosing the radiology images. By incorporating a traceback mechanism and a dynamic learning strategy, our model is compelled to engage in exchange and extract semantic information. Revealing parts of the report apprises the model of the general expression style of the input, thereby concentrating its focus on the alignment of key information. Consequently, this approach results in smaller fluctuations in performance metrics during training and enhances overall performance.

B.3. Limitations

The primary limitation of this study is the elevated computational cost incurred by the additional image decoder and text encoder during the training phase. However, once the multi-modal generation model is fully trained, it becomes feasible to employ pruning techniques to remove components that are irrelevant to specific tasks, such as report generation in our scenario.